

# Consistent boundary conditions for the Yee scheme

Anna-Karin Tornberg<sup>a,b,\*</sup>, Björn Engquist<sup>a,c</sup>

<sup>a</sup> *Royal Institute of Technology (KTH), CSC/Numerical Analysis, SE-100 44 Stockholm, Sweden*

<sup>b</sup> *Courant Institute of Mathematical Sciences, New York University, 251 Mercer Street, New York, NY 10012, USA*

<sup>c</sup> *Department of Mathematics, University of Texas, 1 University Station C1200, Austin, TX 78712, USA*

Received 6 July 2007; received in revised form 31 March 2008; accepted 31 March 2008

Available online 15 April 2008

## Abstract

A new set of consistent boundary conditions for Yee scheme approximations of wave equations in two space dimensions are developed and analyzed. We show how the classical staircase boundary conditions for hard reflections or, in the electromagnetic case, conducting surfaces in certain cases give  $O(1)$  errors. The proposed conditions keep the structure of the Yee scheme and are thus well suited for high performance computing. The higher accuracy is achieved by modifying the coefficients in the difference stencils near the boundary. This generalizes our earlier results with Gustafsson and Wahlund in one space dimension. We study stability and convergence and we present numerical examples.

© 2008 Elsevier Inc. All rights reserved.

*Keywords:* Finite difference time domain (FDTD); Stair-case boundary; Modified coefficients

## 1. Introduction

The Yee scheme for the Maxwell's equations was introduced in 1966, [19] and has since then been the method of choice in many electro-magnetic simulations. This finite difference time domain (FDTD) technique is simply based on centered explicit differencing on staggered grids. We will consider two space dimensions and the TM and TE modes are then given by the following equations, respectively:

$$\begin{aligned}\varepsilon \frac{\partial E_z}{\partial t} &= \frac{\partial H_y}{\partial x} - \frac{\partial H_x}{\partial y}, \\ \mu \frac{\partial H_y}{\partial t} &= \frac{\partial E_z}{\partial x}, \\ \mu \frac{\partial H_x}{\partial t} &= -\frac{\partial E_z}{\partial y},\end{aligned}\tag{1}$$

\* Corresponding author. Address: Courant Institute of Mathematical Sciences, New York University, 251 Mercer Street, New York, NY 10012, USA. Fax: +1 212 995 4121.

*E-mail addresses:* [tornberg@cims.nyu.edu](mailto:tornberg@cims.nyu.edu) (A.-K. Tornberg), [engquist@math.utexas.edu](mailto:engquist@math.utexas.edu) (B. Engquist).

$$\begin{aligned} \mu \frac{\partial H_z}{\partial t} &= \frac{\partial E_x}{\partial y} - \frac{\partial E_y}{\partial x}, \\ \varepsilon \frac{\partial E_y}{\partial t} &= -\frac{\partial H_z}{\partial x}, \\ \varepsilon \frac{\partial E_x}{\partial t} &= \frac{\partial H_z}{\partial y}. \end{aligned} \tag{2}$$

In these equations  $E$ ,  $H$ ,  $\mu$  and  $\varepsilon$  denote the electric and magnetic fields, magnetic permeability and electric permittivity, respectively. We will however use the notation of acoustic waves as was done in the related papers [5,16],

$$\begin{aligned} \frac{\partial p}{\partial t} &= a(x, y) \left( \frac{\partial u}{\partial x} + \frac{\partial v}{\partial y} \right), \\ \frac{\partial u}{\partial t} &= b(x, y) \frac{\partial p}{\partial x}, \\ \frac{\partial v}{\partial t} &= b(x, y) \frac{\partial p}{\partial y}, \end{aligned} \tag{3}$$

where  $(x, y) \in \Omega \subset \mathbb{R}^2$  and  $t > 0$ . Here,  $p$  denotes pressure and  $u$ ,  $v$  the  $x$ - and the  $y$ -velocity components respectively.

Eqs. (1)–(3) are all equivalent. With the substitutions  $p = E_z$ ,  $H_x = -v$  and  $H_y = u$  and  $1/\mu = b$ ,  $1/\varepsilon = a$ , we get (3) from (1), and similarly with the substitutions  $H_z = p$ ,  $E_y = -u$ ,  $E_x = v$  and  $1/\mu = b$ ,  $1/\varepsilon = a$ , we obtain (3) from (2). We will use (3) for the rest of the paper.

Introduce a space step  $\Delta x = \Delta y = h$  and a time step  $\Delta t$ . The Yee scheme is defined on a grid that is staggered in both space and time. The variable  $p$  is stored at half grid points in both  $x$  and  $y$ ,  $(x_{j+1/2}, y_{l+1/2})$  at half time levels  $t^{n+1/2}$ . The  $u$  and  $v$  variables are stored at full time levels  $t^n$ ,  $u$  at full points in  $x$  and half points in  $y$ ,  $(x_j, y_{l+1/2})$ , and  $v$  at half points in  $x$  and full points in  $y$ ,  $(x_{j+1/2}, y_l)$ , as indicated in Fig. 1. Here,  $x_j = jh$ ,  $x_{j+1/2} = (j + 1/2)h$ ,  $y_l = lh$ ,  $y_{l+1/2} = (l + 1/2)h$ , and  $t^n = n\Delta t$ ,  $t^{n+1/2} = (n + 1/2)\Delta t$ .

The Yee scheme for (3) is

$$\begin{aligned} p_{j+1/2, l+1/2}^{n+1/2} &= p_{j+1/2, l+1/2}^{n-1/2} + \Delta t a_{j+1/2, l+1/2} \left( D_{+x} u_{j, l+1/2}^n + D_{+y} v_{j+1/2, l}^n \right) \\ u_{j, l+1/2}^{n+1} &= u_{j, l+1/2}^n + \Delta t b_{j, l+1/2} D_{-x} p_{j+1/2, l+1/2}^{n+1/2}, \\ v_{j+1/2, l}^{n+1} &= v_{j+1/2, l}^n + \Delta t b_{j+1/2, l} D_{-y} p_{j+1/2, l+1/2}^{n+1/2}, \end{aligned} \tag{4}$$

with the difference operators defined by

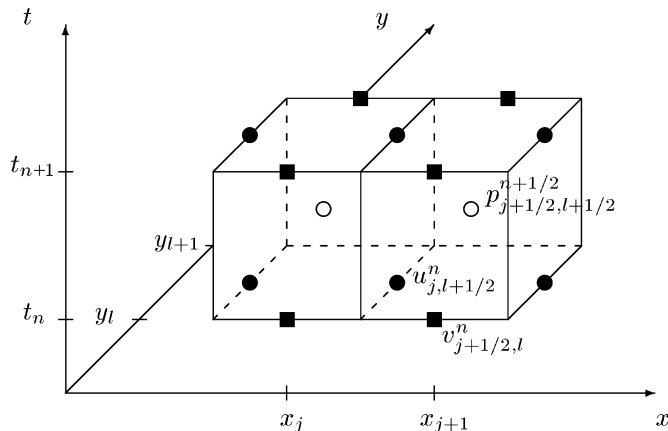


Fig. 1. The staggered grid in space and time.

$$\begin{aligned}
 D_{+x}u_{j,l+1/2} &= (u_{j+1,l+1/2} - u_{j,l+1/2})/h, \\
 D_{+y}v_{j+1/2,l} &= (v_{j+1/2,l+1} - v_{j+1/2,l})/h, \\
 D_{-x}p_{j+1/2,l+1/2} &= (p_{j+1/2,l+1/2} - p_{j-1/2,l+1/2})/h, \\
 D_{-y}p_{j+1/2,l+1/2} &= (p_{j+1/2,l+1/2} - p_{j+1/2,l-1/2})/h.
 \end{aligned}$$

The remarkable success of this FDTD method is based on several virtues. The scheme is second order, explicit and energy conserving. It uses a structured grid, which easily allows for parallel computing and the staggered structure keeps the storage at a minimum.

The natural boundary conditions for (3) is that velocity normal to the boundary vanishes,

$$\hat{\mathbf{n}} \cdot (u, v) = 0, \quad (x, y) \in \Omega, \quad t > 0. \tag{5}$$

This corresponds to the standard PEC boundary conditions for the electromagnetic equations [14]. When the boundary  $\partial\Omega$  is parallel to one of the coordinate axes it is simple to give a consistent numerical boundary conditions. Let, for example,  $\Omega$  be equal to the left half plane. The value of  $p$  closest to the boundary is then updated by a difference formula in which  $u$  to the right is zero. This is the only boundary condition that is needed and it is equivalent to setting the material coefficient  $b$  and the initial values of  $u$  to zero outside the domain. The idea of generating boundary conditions by redefining the coefficients in this context was introduced in [16].

The serious problem comes when the normal of the boundary is not parallel to any coordinate axes. Conditions of the type above are then typically applied locally in a stair-case way, see Fig. 2. In the next section we will give an analytic example for which this standard stair-case boundary approximation generates local  $O(1)$  errors, i.e.  $O(1)$  errors in the solution as measured in the maximum norm. The numerical examples in Sections 4 and 5 further illuminates this problem.

A common technique for resolving the difficulty with the boundary conditions is to use unstructured or conformal grids that are adjusted to match the boundary. See for example [14,7,10] for finite difference and finite element versions of such techniques. However, an FDTD method based on the Yee scheme is attractive since the use of a regular staggered grid is computationally very efficient. Therefore, modifications that are more local in nature have been introduced. One approach is to use a regular grid and the standard Yee scheme for most on the domain, switching to a locally conformal grid only close to the boundaries [2,6,8,11,17,20]. A stable hybrid method, switching from the regular FDTD method to a finite element method close to the boundaries has been designed for the same purpose [13]. In [18], auxiliary points are introduced close to the boundary and skew difference stencils are employed to avoid differencing across the boundary. Extrapolation of field values to grid points falling just outside the domain such that the regular stencils can then be applied is the approach used in [12]. Locally conforming FDTD methods that introduce small irregular cells close to the boundary often suffer from a reduced CFL condition. In [17,20], local modifications that preserves the CFL condition of the original scheme are introduced. All these approaches introduce modifications close to the boundary such that the structure of the Yee scheme is altered. With the structure of the Yee scheme, we here refer to both the regular staggered grid, and the sizes and shapes of the computational stencils. Hence, the use of additional grid values for the update in irregular grid cells alters this structure, even if the grid is kept regular.

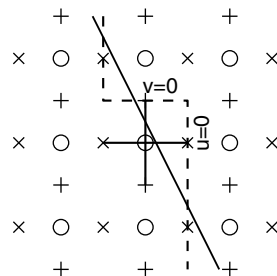


Fig. 2. The boundary  $\Gamma$  given by  $2x + y = h/4$  cutting through the grid, and the corresponding stair-cased boundary (dashed). The stencil for the update of the  $p$ -point in the example is indicated.

It is however possible to keep the structure of the Yee scheme (4) in this strict sense and define consistent boundary conditions for general boundaries by allowing for slightly increased flexibility of the coefficients in (4). In this way the efficiency of the Yee scheme is not affected. The new boundary approximation is derived in Section 3 where we also discuss stability and convergence. The approximation is based on the idea of replacing the boundary conditions by setting material coefficients to zero [16] and the theory of accurate regularization of discontinuous coefficients, [15]. It can be implemented such that the CFL condition for the new scheme is the same as that for the Yee scheme without boundaries. The numerical examples in Sections 4 and 5 show first order convergence in both the maximum norm the discrete 2-norm for these new conditions. It should be mentioned that the error from the boundary and the interior phase error have different characters, see [16]. The phase error increases with time and is often dominant. It is therefore in many simulations acceptable to have lower order approximations at the boundary.

**2. Stair-case boundaries**

Consider the two dimensional Yee scheme (4) for the wave Eq. (3) with the, so-called, stair-case boundary condition at a general boundary. The velocity boundary condition at a solid wall is that the normal component of the velocity is zero, i.e.  $\hat{\mathbf{n}} \cdot \mathbf{u} = 0$  (as given in (5)). The so-called stair-cased boundary condition means that the true boundary is replaced with a stair-cased one, i.e. one with vertical and horizontal line segments only. This stair-cased boundary is placed such that vertical parts of the boundary runs through points where the  $x$ -component of the velocity ( $u$ ) is defined, and here  $u$  is set to zero (the vector normal to this part of the boundary is horizontal). Correspondingly, the horizontal parts of the boundary runs through points where the  $y$ -component of the velocity ( $v$ ) is defined, and here  $v$  is set to zero.

The shortcomings of this treatment has been discussed in a number of publications, [1,3,6–8,12,18]. The general conclusion has often been that the stair-case boundary reduces the accuracy but we have not seen any explicit examples illustrating that the method actually is inconsistent and generically produces  $O(1)$  local errors. One reason for missing the inconsistency may be that the  $0^\circ$ ,  $45^\circ$  and  $90^\circ$  cases are tested and those special cases are consistent as explained in the next section (producing first order errors in both maximum norm and integrated norms). Another reason could be that the standard boundary conditions may still converge in integrated norms even if the convergence is very slow, see Sections 4 and 5.

The following simple counterexample shows that the stair-case boundary condition for the Yee scheme is not consistent and that there are situations that give order one errors after one time step.

Let  $a(x) \equiv b(x) \equiv 1$  and

$$\Omega = \{(x, y) \mid 2x + y < h/4\}, \quad \partial\Omega = \Gamma = \{(x, y) \mid 2x + y = h/4\},$$

which implies  $\hat{\mathbf{n}} = (2, 1)/\sqrt{5}$ , and from the boundary condition  $2u + v = 0$ ,  $(x, y) \in \Gamma$ . The stationary solution  $u(x, y) \equiv 1$ ,  $v(x, y) \equiv -2$  and  $p(x, y) \equiv P$ , for any constant  $P$ , satisfies the equations and the boundary conditions, and we assume that these values are also given as initial conditions. Consider a grid with a  $p$  grid point at  $(0,0)$  a  $u$  point at  $(-h/2, 0)$  and a  $v$  point at  $(0, -h/2)$  with  $\Delta x = \Delta y = h$ , see Fig. 2. The update formula for  $p$  in the first time step will then be based on

$$p^{1/2} = p^{-1/2} + \Delta t((0 - u^0) + (0 - v^0))/h = P + \Delta t/h \neq P.$$

There is thus an immediate  $L_\infty$   $O(1)$  error in after the first update. The numerical examples in Sections 4 and 5 present the character of this type of error in different settings and in different norms.

Our goal in this paper is to keep the boundary approximation as simple as possible and to preserve the important virtues of the interior Yee scheme. We will modify only the coefficients and not the structure of the Yee scheme. We will see later that this modification can be done without affecting the CFL condition of the original scheme.

**3. Derivation of consistent boundary conditions**

Imposing the stair-cased boundary condition is equivalent to setting the material coefficient  $b$  as well as the initial conditions for  $u$  and  $v$  to zero in all points on the stair-cased boundary and outside of the domain. This

idea of generating boundary conditions was introduced in [16], and is convenient for considering modifications to increase the accuracy of the approximation.

Let us consider the equation for  $p$ ,  $p_t = a(u_x + v_y)$ . With the discretization in (4),  $a(u_x + v_y)$  at  $(x, y) = (x_{j+1/2}, y_{l+1/2})$  is approximated by

$$a(u_x + v_y)|_{j+1/2, l+1/2} \approx \frac{1}{h} a_{j+1/2, l+1/2} (u_{j+1, l+1/2} - u_{j, l+1/2} + v_{j+1/2, l+1} - v_{j+1/2, l}).$$

To shorten the notation, we will write this

$$a(u_x + v_y)|_o \approx \frac{1}{h} a_o (u^E - u^W + v^N - v^S),$$

where this notation is also explained in Fig. 3. Here, we assume the material coefficient  $a$  to be constant in the region adjacent to the boundary.

Now, let us assume that the boundary  $\Gamma$  cuts through the stencil such that  $u^E = v^N = 0$  (as depicted in Fig. 4b). We will Taylor expand around a point  $(x^*, y^*)$  on  $\Gamma$ . We get

$$\begin{aligned} \frac{1}{h} a_o (u^E - u^W + v^N - v^S) &= \frac{1}{h} a_o [0 - (u(x^*, y^*) + (x_W - x^*)u_x(x^*, y^*) + (y_W - y^*)u_y(x^*, y^*) + O(h^2)) \\ &+ 0 - (v(x^*, y^*) + (x_S - x^*)v_x(x^*, y^*) + (y_S - y^*)v_y(x^*, y^*) + O(h^2))]. \end{aligned} \tag{6}$$

From Taylor expanding the analytical expression  $a(u_x + v_y)$  at  $\mathbf{x}_o = (x_{j+1/2}, y_{l+1/2})$  around  $(x^*, y^*)$ , we get

$$a(u_x + v_y)|_o = a_o (u_x(x^*, y^*) + v_y(x^*, y^*)) + O(h). \tag{7}$$

To examine the error, we need to compare the expansion in (6) to that in (7). The largest term in (6) is of  $O(1/h)$  and is given by

$$\frac{1}{h} a_o (-u(x^*, y^*) - v(x^*, y^*)).$$

There is no corresponding term in (7), and we need to examine if this term vanishes.

Let  $\Gamma^*$  be the line tangent to  $\Gamma$  at  $(x^*, y^*)$ , and denote the angle of  $\Gamma^*$  to the  $x$ -axis by  $\alpha$  ( $0 \leq \alpha \leq \pi$ ). Introduce the coordinate system  $(\xi, \eta)$ , where  $\xi$  is along  $\Gamma^*$ . In this coordinate system,  $\mathbf{u} = \tilde{u}\tilde{\xi} + \tilde{v}\tilde{\eta}$  with the boundary condition  $\mathbf{u} \cdot \hat{\mathbf{n}} = \tilde{v} = 0$  on  $\Gamma$ .

We have

$$u = \cos \alpha \tilde{u} + \sin \alpha \tilde{v}, \quad v = \sin \alpha \tilde{u} + \cos \alpha \tilde{v},$$

and hence

$$\frac{1}{h} a_o (-u(x^*, y^*) - v(x^*, y^*)) = \frac{1}{h} a_o (-\cos \alpha + \sin \alpha) \tilde{u}(\xi^*, \eta^*),$$

where we have used the fact that  $\tilde{v}(\xi^*, \eta^*) = 0$ , where  $(\xi^*, \eta^*)$  are the coordinates for the point  $(x^*, y^*)$  in the  $\xi - \eta$  coordinate system.

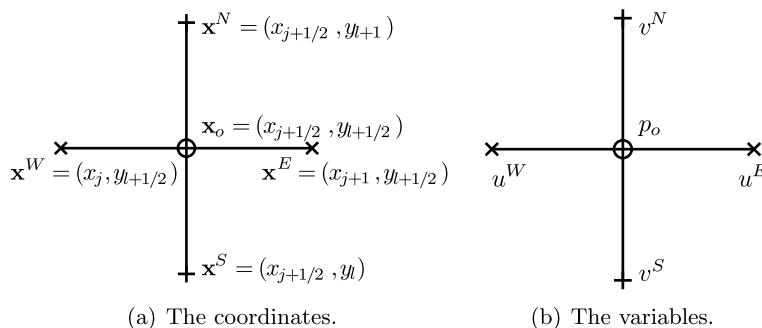


Fig. 3. The points in the stencil for the update of  $p$  (i.e. the evaluation of  $a(u_x + v_y)$ ) at  $\mathbf{x}_o = (x_{j+1/2}, y_{l+1/2})$ .

Indeed, with the exception of the special case of  $\alpha = 3\pi/4$  (within the range of angles for which the stencil could be cut this way), this term does not vanish and is in general  $O(1/h)$ . Hence, the error in the numerical approximation of  $a(u_x + v_y)$  at a point with a stencil intersecting the boundary is  $O(1/h)$ . Since in the formula (4) for updating  $p$  the approximation of  $a(u_x + v_y)$  is multiplied by  $\Delta t$  the error in  $p$  already after one time step may be  $O(1)$ . See also the example in Section 2.

The Yee scheme was introduced in (4). With this discretization, we can not modify the  $a$ -coefficient to improve on the discretization, since it is multiplying the whole expression. Let us instead introduce the modified discretization

$$\begin{aligned} p_{j+1/2, l+1/2}^{n+1/2} &= p_{j+1/2, l+1/2}^{n-1/2} + \Delta t a_{j+1/2, l+1/2} \left( D_{+x} \left( c_{j, l+1/2}^{(1)} u_{j, l+1/2}^n \right) + D_{+y} \left( c_{j+1/2, l}^{(2)} v_{j+1/2, l}^n \right) \right), \\ u_{j, l+1/2}^{n+1} &= u_{j, l+1/2}^n + \Delta t b_{j, l+1/2} D_{-x} p_{j+1/2, l+1/2}^{n+1/2}, \\ v_{j+1/2, l}^{n+1} &= v_{j+1/2, l}^n + \Delta t b_{j+1/2, l} D_{-y} p_{j+1/2, l+1/2}^{n+1/2}, \end{aligned} \tag{8}$$

and let us write

$$a(u_x + v_y)|_o \approx \frac{1}{h} (\tilde{a}^E u^E - \tilde{a}^W u^W + \tilde{a}^N v^N - \tilde{a}^S v^S). \tag{9}$$

This is the approximation of  $a(u_x + v_y)$  in  $(x, y) = (x_{j+1/2}, y_{l+1/2})$  in the scheme (8) with  $\tilde{a}^E = a_{j+1/2, l+1/2} c_{j+1, l+1/2}^{(1)}$ ,  $\tilde{a}^W = a_{j+1/2, l+1/2} c_{j, l+1/2}^{(1)}$ ,  $\tilde{a}^N = a_{j+1/2, l+1/2} c_{j+1/2, l+1}^{(2)}$ , and  $\tilde{a}^S = a_{j+1/2, l+1/2} c_{j+1/2, l}^{(2)}$ . With this, following the same steps as above, we get that the  $O(1/h)$  term in the expansion is given by

$$\frac{1}{h} (-\tilde{a}^W u(x^*, y^*) - \tilde{a}^S v(x^*, y^*)) = \frac{1}{h} (-\tilde{a}^W \cos \alpha + \tilde{a}^S \sin \alpha) \tilde{u}(x^*, y^*).$$

This term can be made to vanish by choosing  $c^{(1)}$  and  $c^{(2)}$  and thus  $\tilde{a}^W$  and  $\tilde{a}^S$  appropriately, such that

$$\tilde{a}^W \cos \alpha + \tilde{a}^S \sin \alpha = 0. \tag{10}$$

If this term is made to vanish, the leading order term in the expansion improves with one order and is  $O(1)$ , as given by

$$-\frac{\tilde{a}_W}{h} ((x_W - x^*)u_x(x^*, y^*) + (y_W - y^*)u_y(x^*, y^*)) - \frac{\tilde{a}_S}{h} ((x_S - x^*)v_x(x^*, y^*) + (y_S - y^*)v_y(x^*, y^*)).$$

This should match the  $O(1)$  term in (7),  $a_o(u_x(x^*, y^*) + v_y(x^*, y^*))$ . With only  $\tilde{a}_W$  and  $\tilde{a}_S$  to be determined, we are not able to fulfill both the consistency condition (10) and to match this  $O(1)$  term. Hence, with this structure of the scheme, with only two  $u$  and two  $v$  points in the stencil, we can do no better than to eliminate the very largest error by fulfilling the consistency condition (10). This implicates that we will still have an  $O(h)$  error in the numerical solution after one time step, and we should expect a first order error in the numerical solution to the PDE.

The way the stair-cased boundary is placed in the grid implies that there are no difference formulas for  $bp_x$  or  $bp_y$  intersecting this boundary.

The consistency condition that needs to be fulfilled to avoid an  $O(1)$  maximum norm error in the solution to the PDE depends on the manner in which the boundary intersects the computational stencil. In Fig. 4, the four cases where the boundary is intersecting the computational stencil in both  $x$  and  $y$  are indicated. In Fig. 5, the four cases where the boundary is intersecting the computational stencil either only in  $x$  or only in  $y$  are indicated. The consistency conditions are summarized in Table 1. Note that for  $\Gamma$  a straight line at an angle  $\alpha = 0, \pi/4, \pi/2$  or  $3\pi/4$  are special cases, where  $a^N = a^S = a^W = a^E = a$  obeys the corresponding consistency condition.

There are also cases where the physical boundary falls outside of the computational stencil, but where the  $b$ -coefficient in one  $u$ -point and/or one  $v$ -point has been set to zero to define the stair-cased boundary. Such cases can also be categorized by the cases depicted in Figs. 4 and 5 with the corresponding consistency conditions listed in Table 1, using the values of the  $b$ -coefficients to define inside/outside. The only difference is that the

point  $(x^*, y^*)$  on  $\Gamma$ , at which we define  $\alpha$  from the slope of the tangent line, will now fall outside of the  $h \times h$  square defined by the computational stencil. The stair-cased boundary definition will also modify any case where  $\Gamma$  intersects one axes of the computational stencil more than once, and hence, the cases given above are all the cases that we need to consider.

### 3.1. Implementation

The implementation of the modified coefficients involves two main steps: First, the  $b$ -coefficients should be set to zero in points outside the actual domain, but also in some extra points such as to define the stair-cased boundary. Doing only this results in the original stair-cased grid approximation, i.e. it is equivalent to setting  $u$  and  $v$  equal to zero at vertical and horizontal parts of the stair-cased boundary, respectively.

Once the  $b$ -coefficients have been modified, it is time to modify the coefficients in the stencil for the pressure update. To do this, we need to identify “irregular” points for this update, i.e. where the computational stencil is intersected by the stair-cased boundary. This means that the update involves  $u$  and/or  $v$  both at points where  $b$  holds its interior value, and where it has been set to zero.

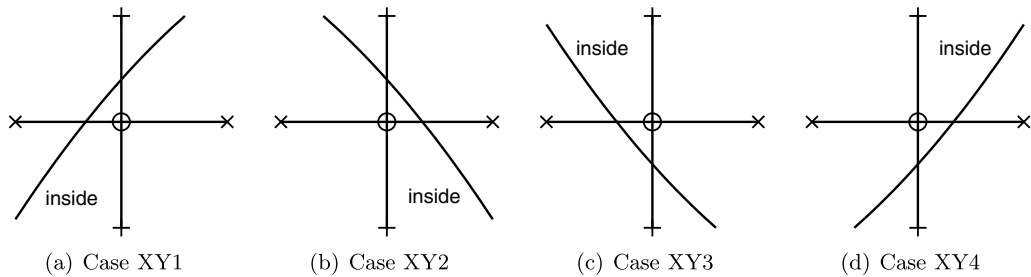


Fig. 4. The four different cases for a stencil intersected in both the  $x$  and  $y$  direction.

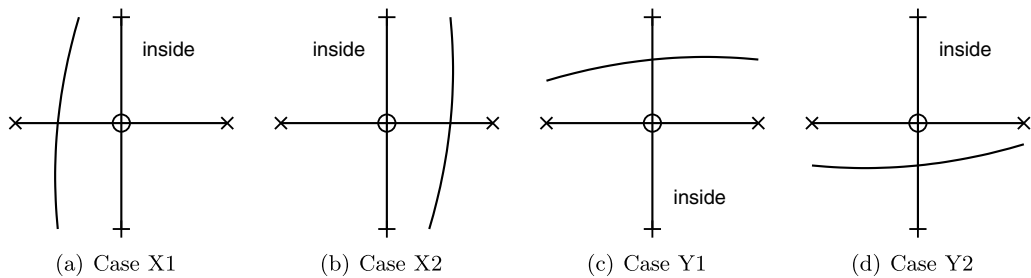


Fig. 5. The four different cases for a stencil intersected in either only the  $x$  or the  $y$  direction.

Table 1

The consistency conditions for the different cases sketched in Figs. 4 and 5, with the notation as given in (9)

Case	Consistency condition
XY1	$\tilde{a}^E \cos \alpha - \tilde{a}^S \sin \alpha = 0$
XY2	$\tilde{a}^W \cos \alpha + \tilde{a}^S \sin \alpha = 0$
XY3	$\tilde{a}^E \cos \alpha + \tilde{a}^N \sin \alpha = 0$
XY4	$\tilde{a}^W \cos \alpha - \tilde{a}^N \sin \alpha = 0$
X1	$\tilde{a}^E \cos \alpha + (\tilde{a}^N - \tilde{a}^S) \sin \alpha = 0$
X2	$\tilde{a}^W \cos \alpha - (\tilde{a}^N - \tilde{a}^S) \sin \alpha = 0$
Y1	$(\tilde{a}^E - \tilde{a}^W) \cos \alpha - \tilde{a}^S \sin \alpha = 0$
Y2	$(\tilde{a}^E - \tilde{a}^W) \cos \alpha + \tilde{a}^N \sin \alpha = 0$

The angle  $\alpha$  is the angle to the  $x$ -axis of the line tangent to the boundary  $\Gamma$  at the point  $(x^*, y^*)$  ( $0 \leq \alpha < \pi$ ). Note: the point  $(x^*, y^*)$  can be any point on the boundary within the  $h \times h$  square defined by the computational stencil. A different choice only affects the next order term in the expansion, and not the consistency condition.

After the irregular points have been identified, we must for each point define the modified coefficients, i.e. we will determine  $\tilde{a}^E$ ,  $\tilde{a}^W$ ,  $\tilde{a}^N$  and  $\tilde{a}^S$ , such that the applicable condition in Table 1 is fulfilled. This consistency condition does not however completely determine these coefficients. We choose the coefficients such that each of them takes a value between zero and the original value of  $a$ , such as not to affect the CFL condition for the scheme. As an example, consider case XY1. Here,  $\alpha$  should lie in the range between 0 and  $\pi/2$  for the curve to intersect the stencil in this manner. If  $\alpha \leq \pi/4$ , we let  $\tilde{a}^S = a$ , and set  $\tilde{a}^E = (\sin \alpha / \cos \alpha) \tilde{a}^S$ , and if  $\alpha > \pi/4$  we instead set  $\tilde{a}^E = a$ , and set  $\tilde{a}^S = (\cos \alpha / \sin \alpha) \tilde{a}^E$ . Similarly, for each case listed in Table 1, there is only one of the  $a$ -coefficients that will be modified, which one depends on the value of  $\alpha$ . This is given in Tables 18 and 19 in Appendix.

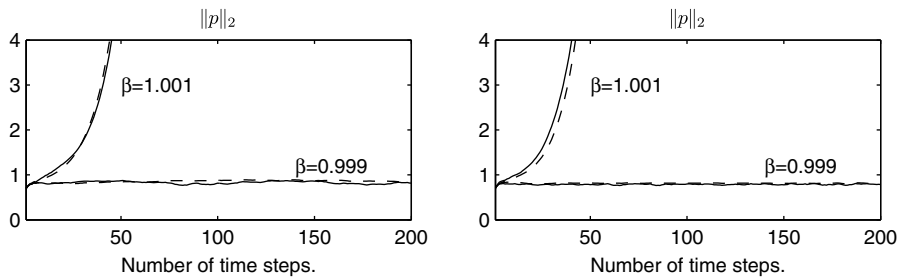
If the boundary  $\Gamma$  is a straight line cutting through the grid,  $\alpha$  is given by the angle of that line to the  $x$ -axis ( $0 \leq \alpha < \pi$ ). If  $\Gamma$  is some other curve, a point  $(x^*, y^*)$  on the curve must be selected, and  $\alpha$  for the tangent line at that point computed. This is further discussed in Appendix.

Remember that the exact choice of  $(x^*, y^*)$  does not affect the consistency condition. These coordinates would however explicitly enter any conditions imposed to eliminate higher order error terms.

### 3.2. Stability and convergence

In [5] a discrete stability  $L^2$  estimate for (4) with variable coefficients is derived. With the more general form (8) we have to rely on numerical investigations in order to study the stability. In a set of numerical experiments with different geometries the discrete  $L^2$  norm did not increase with time for random initial data when the step sizes were bounded by an appropriate CFL condition. Furthermore, in all tests, our new numerical scheme with modified coefficients experiences the same CFL condition as the Yee scheme for problems without boundaries, which for coefficients that are constant in the interior is  $\Delta t/h \leq 1/\sqrt{2ab}$ , [5]. This is illustrated in Fig. 6. The discrete  $L^2$ -norm of  $p$  is plotted versus the number of time steps for a time step size slightly below and slightly above this CFL condition. This is done for two different choices of the boundary  $\Gamma$ : a straight inclined boundary and an enclosed cylinder. Here,  $p$ ,  $u$  and  $v$  are in each grid point initialized by a random number between 0 and 1 (uniform distribution). Any numerical instability will with these initial conditions grow much sooner than for smooth initial data. The system is discretized on the domain  $[0, 2\pi] \times [0, 2\pi]$ , with a spatial step size  $\Delta x = \Delta y = h = 2\pi/N$ . The plots clearly illustrate that when the time step obeys the CFL condition, the norm of the solution is bounded, where as it grows rapidly as soon as the time step exceeds the CFL condition. Again, we emphasize that this is the same CFL condition as for the problem without any boundaries, even though the boundary cuts the computational cells into many different ratios.

The error analysis used for the derivation in Section 3 shows that the local truncation error for the modified scheme is bounded by a constant at boundary points and  $O(h^2)$  in the interior. Since the number of boundary points is  $O(1/h)$  the discrete  $L^2$  norm of the local truncation error is of order  $O(h^{1/2})$  and  $L^2$  stability would then imply consistency with convergence rate  $O(h^{1/2})$ . The result by Gustafsson in [4] is often cited as having established that there is a gain of one order of accuracy in influence from the truncation error at the boundary



(a)  $\Gamma$  a straight line given by (17), with  $\alpha = \pi/6$  and  $\bar{x} = \sqrt{2}\pi/30$ . (b)  $\Gamma$  a circle of radius  $R = 8\pi/30$ , centered in  $(\bar{x}, \bar{y}) = (1 + \pi/700, 1 - \sqrt{2}/200)\pi$ .

Fig. 6. The discrete  $L^2$ -norm of  $p$  plotted versus the number of time-steps for  $N = 80$  (solid) and  $N = 240$  (dashed) for different values of  $\beta$ . The time-step  $\Delta t = \beta h / \sqrt{2ab}$ , where  $\beta = 1$  is the CFL limit for the Yee scheme for problems without boundaries.



to the global error. Even if our case is not covered by that theory, all numerical examples in Sections 4 and 5 clearly show a first order global convergence rate. See also [14] for a discussion on this matter.

**Remark.** The following example shows that it is in general impossible to achieve more than first order accuracy even with the generalized Yee type of algorithm with

$$p_{j+1/2,l+1/2}^{n+1/2} = p_{j+1/2,l+1/2}^{n-1/2} + \frac{\Delta t}{h} (\tilde{a}_E u_{j+1,l+1/2}^n - \tilde{a}_W u_{j,l+1/2}^n + \tilde{a}_N v_{j+1/2,k+1}^n - \tilde{a}_S v_{j+1/2,k}^n).$$

Let

$$\Omega = \{(x, y) \mid x + y < h/4\}, \quad \partial\Omega = \Gamma = \{(x, y) \mid x + y = h/4\},$$

which implies  $\hat{\mathbf{n}} = (1, 1)/\sqrt{2}$ , and  $u + v = 0$  for  $(x, y) \in \partial\Omega$ .

Consider a grid with a  $p$  grid point at  $(0, 0)$ , a  $u$  point at  $(-h/2, 0)$  and a  $v$  point at  $(0, -h/2)$ . The update formula for  $p$  will then be based on

$$p_{j+1/2,l+1/2}^{n+1/2} = p_{j+1/2,l+1/2}^{n-1/2} + \frac{\Delta t}{h} (\tilde{a}_E u_{j+1,l+1/2}^n - \tilde{a}_S v_{j+1/2,k}^n),$$

where the different  $a$ -coefficients are possible in the generalized Yee scheme.

If we now take  $u(x, y, 0) = h/2 + x - 5y$  and  $v(x, y, 0) = h/2 - 5x + y$ , this choice satisfies the boundary condition and the  $u_x - v_y \equiv 0$  condition (the vorticity is invariant under evolution of Eq. (3)). The value of  $p_{j+1/2,l+1/2}^{n+1/2} - p_{j+1/2,l+1/2}^{n-1/2}$  ( $n = 0$ ) should be  $2\Delta t$  but the update formula gives 0. This implies that there is a  $O(h)$  error in  $p$  immediately after the update.

To avoid this  $O(h)$  error in  $p$ , we need to eliminate not only the  $O(1/h)$  but also the  $O(1)$  error term in the approximation of  $a(u_x + v_y)$ . To do so, the two degrees of freedom we have in choosing  $\tilde{a}^E$  and  $\tilde{a}^S$  are not sufficient and hence this cannot be done without altering the structure of the Yee scheme. This is in contrast to the one-dimensional case, where all solution components are continuous, and global second order convergence can be obtained with only a modification of the coefficients [15].

## 4. Test Case I: A straight inclined boundary

### 4.1. Constant solutions

Certainly, no numerical method is needed to compute a solution that is constant in both space and time. But in this context it is valuable to consider such a trivial solution to highlight the errors introduced by the original stair-cased boundary approximation.

The boundary conditions at a solid wall are  $\hat{\mathbf{n}} \cdot \nabla p = 0$  and  $(u, v) \cdot \hat{\mathbf{n}} = 0$ , where  $\hat{\mathbf{n}}$  is the vector normal to the boundary. For a straight inclined boundary, making an angle  $\alpha = \arctan(1/d)$  to the  $x$ -axis, the normal vector is  $(-1, d)/\sqrt{1+d^2}$ , and the velocity boundary condition is  $-u + dv = 0$ . Hence,  $u = 1$ ,  $v = 1/d$  and  $p = P$  for any constant  $P$  is a solution to (3) with these boundary conditions (5).

It was already noted in Section 2, that with the original stair-cased approximation, there is an  $O(1) L^\infty$  error for  $p$  already after the first time step (that example was for the case  $d = -1/2$ ).

With the modifications of the coefficients, such that the consistency conditions in Table 1 are fulfilled, there is no error for any  $\alpha$  in the numerical approximation in this case. The solution  $u = 1$ ,  $v = 1/d$  and  $p = P$  is an exact solution also to the numerical approximation.

Before we proceed to the more general case of an incoming wave that is being reflected at the boundary, we will study the errors for the stair-cased approximation in this very simple case. For the special case of  $d = \pm 1$ , i.e.  $\alpha = \pi/4$  and  $3\pi/4$ , respectively, the stair-cased boundary approximation obeys the consistency conditions, and there are no errors in the approximation of these constant solutions. This is also true for a vertical or a horizontal boundary. (The original stair-cased approximation and the modified approximation coincide in these cases).

The Yee scheme is staggered not only in space, but also in time, i.e. the numerical approximations of  $u$  and  $v$  are available at times  $t_n = n\Delta t$ , and  $p$  at times  $t_{n+1/2} = (n + 1/2)\Delta t$ . We want to be able to measure the error for

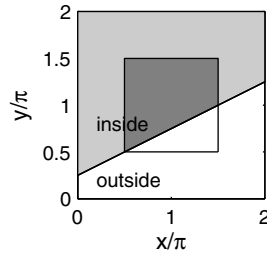


Fig. 7. The computational domain with an inclined boundary with  $\alpha = \arctan(1/2)$ . The area in grey is inside the physical domain. The numerical errors are measured in  $\bar{\Omega}$ : the part of the region  $[\pi/2, 3\pi/2] \times [\pi/2, 3\pi/2]$  that falls inside the physical domain (colored dark grey in the picture).

different grid resolutions at the same points in time. To have the numerical solutions for both  $u, v$  and  $p$  available at common points in time, we use a grid refinement factor of 3.

We solve the problem on  $[0, 2\pi] \times [0, 2\pi]$  with periodic outer boundary conditions. The coefficients are  $a = b = -1$ . We define the inclined boundary by  $Y(x) = (x - \bar{x}) \tan(\alpha) = (x - \bar{x})/d$ , with  $\bar{x} = (1 - d)\pi/2$ , that divides the square into two parts; inside to the left and outside to the right. In order not to include errors from the outer boundaries in our measurements, we measure the errors over an inner area  $\bar{\Omega}$ , as indicated in Fig. 7, and compute up to a limited time. The errors are measured both in maximum norm, and in the discrete  $L^2$ -norm. These norms are for a grid function  $f$  defined in grid points  $(x_{j+1/2}, y_{l+1/2})$  defined as

$$\|f\|_\infty = \max_{j,l \in J_p} |f_{j+1/2,l+1/2}|, \quad \|f\|_2 = \left( \frac{1}{N_p} \sum_{j,l \in J_p} |f_{j+1/2,l+1/2}|^2 \right)^{1/2}. \tag{11}$$

Here,  $J_p$  is the set of indices  $(j, l)$  for which the grid points  $(x_{j+1/2}, y_{l+1/2})$  fall inside the check area  $\bar{\Omega}$ , and  $N_p$  are the number of such grid points. The norms for grid functions defined in points  $(x_j, y_{l+1/2})$  and  $(x_{j+1/2}, y_l)$  are defined analogously.

In the following we have used three grid resolutions, with the number of grid points in each dimension  $N = 100, 300$  and  $900$ . Hence,  $h = 2\pi/N$ , and we set  $\Delta t = 0.6h$ .

In Tables 2 and 3, we present the results for  $d = 2$ . From these results, we can see that there is no convergence in maximum norm for  $u$  and  $v$ , while we measure a convergence order of 0.3 for  $p$ . Hence, for  $u$  and  $v$ , there is an  $O(1)$  error in maximum norm, for this very simple constant solution.

Table 2

Error for the stair-cased approximation in maximum norm and computed convergence rate  $q$  for  $u, v$  and  $p$  at  $t = 0.3\pi$  with  $\alpha = \arctan(1/2)$

$N$	$u$		$v$		$p$	
	Error	$q$	Error	$q$	Error	$q$
100	0.3027	–	0.2162	–	0.1173	–
300	0.3068	–0.12	0.1897	0.12	0.0898	0.24
900	0.3091	–0.01	0.1914	–0.01	0.0628	0.32

The exact solution is  $u \equiv 1, v \equiv 1/2, p \equiv 0$ .

Table 3

As Table 2, but with the error measured in discrete  $L^2$ -norm

$N$	$u$		$v$		$p$	
	Error	$q$	Error	$q$	Error	$q$
100	0.0362	–	0.0356	–	0.0330	–
300	0.0218	0.46	0.0201	0.52	0.0192	0.49
900	0.0126	0.50	0.0116	0.50	0.0111	0.50

These  $O(1)$  errors are created at the stair-cased boundary, and propagate out in the domain. As they do so, their magnitude decrease, and measuring the error in the  $L^2$  norm, we see a  $h^{1/2}$  convergence, for all of  $u$ ,  $v$  and  $p$ . This is a typical behaviour for an arbitrary choice of  $d$  (excluding the special cases mentioned above). As also mentioned above, with modified coefficients, the numerical solution is exact for all choices of  $d$ .

#### 4.2. Time harmonic solutions

We can write the system in (3) as

$$\frac{\partial p}{\partial t} = a(\nabla \cdot \mathbf{u}), \quad (12)$$

$$\frac{\partial \mathbf{u}}{\partial t} = b \nabla p, \quad (13)$$

where  $\mathbf{u} = (u, v)$ . Let us consider a complex valued velocity potential  $V(\mathbf{x}, t)$ , and define

$$p = \frac{1}{b} \Re \left( \frac{\partial V}{\partial t} \right), \quad \mathbf{u} = \Re(\nabla V), \quad (14)$$

where  $\Re(\cdot)$  indicates the real part. With this, (13) is automatically fulfilled, and (12) becomes

$$\frac{\partial^2 V}{\partial t^2} = ab \nabla^2 V = c^2 \nabla^2 V.$$

For a velocity potential with harmonic time dependence,

$$V(x, y, t) = \Psi(x, y) e^{-i\omega t}, \quad (15)$$

this becomes

$$(\nabla^2 + k^2) \Psi = 0, \quad (16)$$

where  $k = \omega/c$ . Requiring  $\hat{\mathbf{n}} \cdot \nabla \Psi = \partial \Psi / \partial n = 0$  at the solid wall, our boundary conditions  $\hat{\mathbf{n}} \cdot \mathbf{u} = 0$  and  $\partial p / \partial n = 0$  are satisfied (according to the definitions in (14)).

Consider an inclined boundary  $\Gamma$  that makes an angle  $\alpha$  to the  $x$ -axis. For  $0 < \alpha < \pi$  we define  $\Gamma$  by

$$\Gamma = \{(x, y) : x \in \mathbb{R}, y = Y(x) = (x - \bar{x}) \tan \alpha\}. \quad (17)$$

For an incoming plane wave  $e^{ikx}$  that is reflected in the boundary, the solution is

$$\Psi(x, y) = e^{ikx} + e^{ikx^*} \cdot e^{ik((x-x^*) \cos 2\alpha + (y-y^*) \sin 2\alpha)}, \quad (18)$$

where  $(x^*, y^*)$  is any point on the boundary  $\Gamma$ . From this, the pressure and velocity components are defined by (14) together with (15). Hence,

$$p(x, y, t) = \frac{1}{b} \Re(-i\omega \Psi(x, y) e^{-i\omega t}), \quad \mathbf{u}(x, y, t) = (u(x, y, t), v(x, y, t)) = \Re(\nabla \Psi(x, y) e^{-i\omega t}), \quad (19)$$

where  $\Psi(x, y)$  is given in (18).

One example of an analytical time harmonic solution for  $p$  is shown in Fig. 8, where also the incoming and reflected contribution to the total solution are shown. Fig. 9 displays the corresponding analytical solution for the velocity components  $u$  and  $v$ . Note that  $v \equiv 0$  for the incoming wave, and there is only a vertical velocity component for the reflected wave.

#### 4.3. Numerical results

We will present numerical results for an incoming plane wave being reflected at an inclined boundary at an angle of  $\alpha = \pi/6$ ,  $\pi/4$  and  $3\pi/8$ . For all results given in this section, we set the wave number of the incoming wave to  $k = \omega/c = 5$ .

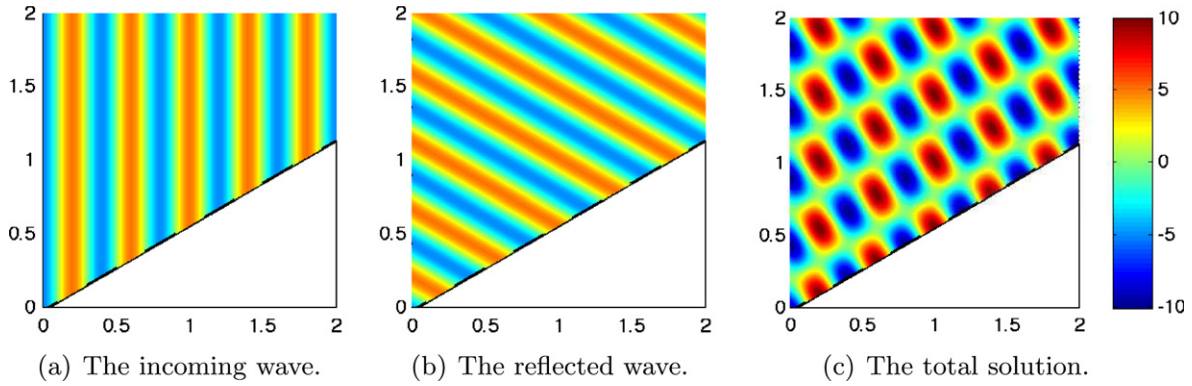


Fig. 8. The analytical solution for  $p$  at  $t = 0.3\pi$  for an incoming wave with wave number  $k = 5$ .  $\alpha = \pi/6$ ,  $\bar{x} = 0.05\pi$ .

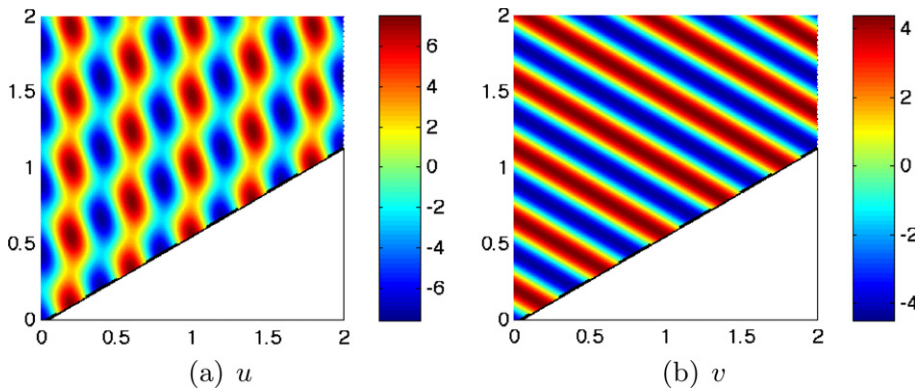


Fig. 9. The analytical solution for  $u$  and  $v$  at  $t = 0.3\pi$ .  $k = 5$ ,  $\alpha = \pi/6$  and  $\bar{x} = 0.05\pi$ .

As in the constant solution case (Section 4.1), we will use a refinement factor of 3, grid resolutions  $N = 100, 300$  and  $900$ , and  $\Delta t = 0.6h$ , where  $h = 2\pi/N$ . For each  $\alpha$ , we will set a  $\bar{x}_0$ , and then for each resolution perform  $M = 6$  runs, with the  $\Gamma$  defined by (17) with  $\bar{x} = \bar{x}_j$ ,  $j = 1, \dots, M$ ,

$$\bar{x}_j = \bar{x}_0 + h \frac{\sqrt{2}}{1.42} \frac{j - 1}{M - 1}. \tag{20}$$

The errors are measured in both maximum norm and the discrete  $L^2$ -norm as compared to the analytical solution over the part of the region  $[\pi/2, 3\pi/2] \times [\pi/2, 3\pi/2]$  that also falls inside the physical domain. This is to avoid to measure errors that occur at the outer boundaries. The errors presented in the tables below are the largest errors incurred for the  $M = 6$  shifts in the grid.

The analytical and numerical solutions for  $p$ ,  $u$  and  $v$  for the first shift ( $j = 1$ ) in (20) for are shown in Figs. 10–12. From these plots, we can see the lower quality of the numerical solution obtained with the original stair-cased approximation for example in the form of numerical oscillations.

In Tables 4–13, the errors in the numerical results and the convergence rates are given in both maximum norm and  $L^2$ -norm for different angles of the inclined boundary ( $\alpha = \pi/6, \pi/4$  and  $3\pi/8$ ), both for the original stair-cased approximation and with modified coefficients (in the  $\alpha = \pi/4$  case these approximations coincide). The results for  $\alpha = \pi/6$  are found in Tables 4–7, for  $\alpha = \pi/4$  in tables 8–9, and  $\alpha = 3\pi/8$  in Tables 10–13.

As in the case for the constant solution, we can note that with this original stair-cased approximation, there is an  $O(1)$  error in maximum norm for both  $u$  and  $v$ , both for  $\alpha = \pi/6$  and  $\alpha = 3\pi/8$  (Tables 4 and 10). The convergence rates measured in the discrete  $L^2$ -norm (Tables 5 and 11) are somewhat higher than the  $q = 0.5$  that was so clearly measured for the constant solution case (Tables 2 and 3).

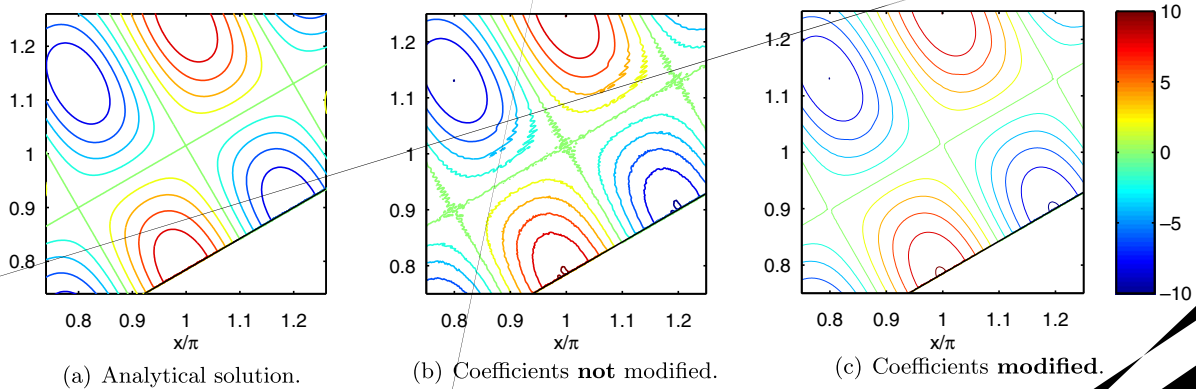


Fig. 10. The solution for  $p$  at  $t = 0.3\pi$  displayed in a smaller part of the domain.  $N = 900$  for the numerical solutions.  $\alpha = 0.1$  and  $\bar{x} = \pi(1 - \sqrt{3} + \sqrt{2}/100)/2$ .

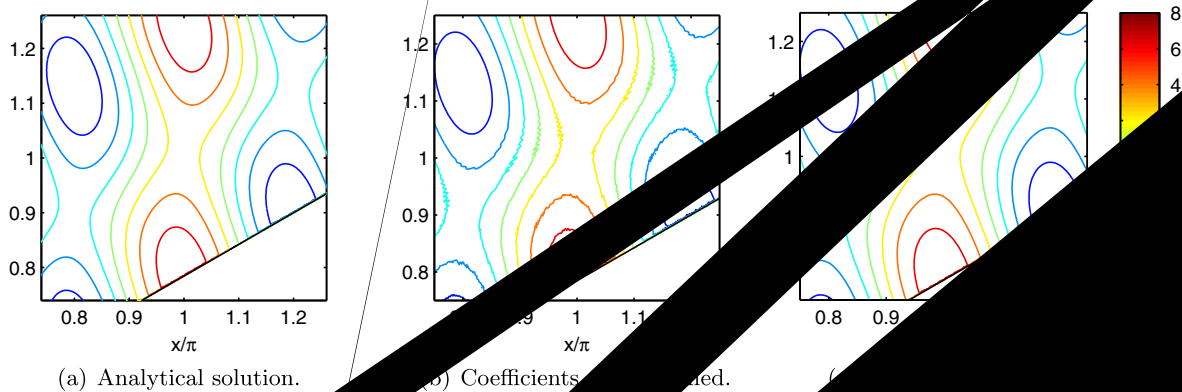


Fig. 11. The same as Fig. 10 but for  $u$ .

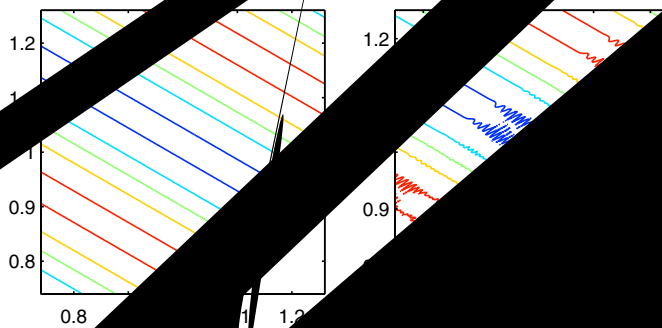
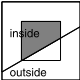


Table 4  
Error in maximum norm and computed convergence rate  $q$  at  $t = 0.3\pi$  for  $u$ ,  $v$  and  $p$

$N$	$u$		$v$		$p$	
	Error	$q$	Error	$q$	Error	$q$
100	2.7452	–	3.1743	–	2.9880	–
300	2.7534	–0.003	2.3823	0.26	0.9832	1.01
900	2.6460	0.036	2.1402	0.10	0.5721	0.49

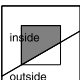


$\alpha = \pi/6$   
 $\bar{x}_0 = \frac{\pi}{2} (1 - \sqrt{3} + \frac{\sqrt{2}}{100})$

The coefficients have **not** been modified. Error given is taken as the maximum over  $M = 6$  shifts in the grid according to (20).

Table 5  
As Table 4 (coefficients **not** modified) but for errors measured in the discrete  $L^2$ -norm

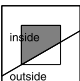
$N$	$u$		$v$		$p$	
	Error	$q$	Error	$q$	Error	$q$
100	0.3487	–	0.3921	–	0.4709	–
300	0.1552	0.74	0.1486	0.88	0.1642	0.96
900	0.0786	0.62	0.0708	0.67	0.0722	0.75



$\alpha = \pi/6$   
 $\bar{x}_0 = \frac{\pi}{2} (1 - \sqrt{3} + \frac{\sqrt{2}}{100})$

Table 6  
As Table 4 (errors in maximum norm) but for **modified** coefficients

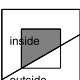
$N$	$u$		$v$		$p$	
	Error	$q$	Error	$q$	Error	$q$
100	1.1016	–	1.8450	–	2.5077	–
300	0.4273	0.86	0.5608	1.08	0.6507	1.23
900	0.1402	1.01	0.1794	0.10	0.2069	1.04



$\alpha = \pi/6$   
 $\bar{x}_0 = \frac{\pi}{2} (1 - \sqrt{3} + \frac{\sqrt{2}}{100})$

Table 7  
As Table 4 but for **modified** coefficients with errors measured in discrete  $L^2$ -norm

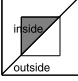
$N$	$u$		$v$		$p$	
	Error	$q$	Error	$q$	Error	$q$
100	0.2757	–	0.3842	–	0.4906	–
300	0.0964	0.96	0.1212	1.05	0.1519	1.07
900	0.0328	0.98	0.0396	1.02	0.0494	1.02



$\alpha = \pi/6$   
 $\bar{x}_0 = \frac{\pi}{2} (1 - \sqrt{3} + \frac{\sqrt{2}}{100})$

Table 8  
Error in maximum norm and computed convergence rate  $q$  at  $t = 0.3\pi$  for  $u, v$  and  $p$

$N$	$u$		$v$		$p$	
	Error	$q$	Error	$q$	Error	$q$
100	0.7044	–	1.0515	–	1.7318	–
300	0.2949	0.79	0.3938	0.89	0.5935	0.97
900	0.0929	1.05	0.1070	1.19	0.1678	1.15

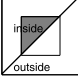


$\alpha = \pi/4$   
 $\bar{x}_0 = \sqrt{2}\pi/200$

For this special case of  $\alpha = \pi/4$ , the modified and the not modified coefficients coincide. Error is taken as the maximum over 6 shifts in the grid according to (20).

Table 9  
As in Table 8 but with the error measured in the discrete  $L^2$ -norm

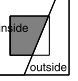
$N$	$u$		$v$		$p$	
	Error	$q$	Error	$q$	Error	$q$
100	0.2025	–	0.3097	–	0.4662	–
300	0.0744	0.91	0.1114	0.93	0.1645	0.95
900	0.0258	0.96	0.0309	1.17	0.0469	1.14



$\alpha = \pi/4$   
 $\bar{x}_0 = \sqrt{2}\pi/200$

Table 10  
Error in maximum norm and computed convergence rate  $q$  at  $t = 0.3\pi$  for  $u, v$  and  $p$

$N$	$u$		$v$		$p$	
	Error	$q$	Error	$q$	Error	$q$
100	1.4345	–	1.7683	–	1.2059	–
300	1.1369	0.21	1.4016	0.21	0.4598	0.88
900	1.1130	0.02	1.3805	0.01	0.3409	0.27



$\alpha = 3\pi/8$   
 $\bar{x}_0 = \frac{3\pi}{2}(2 - 1.01\sqrt{2})$

The coefficients have **not** been modified. The error is taken as the maximum over  $M = 6$  shifts in the grid according to (20).

## 5. Test Case II: A cylinder

### 5.1. Time harmonic solutions

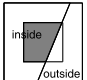
Consider a cylinder, centered in  $(\bar{x}, \bar{y})$  with radius  $R$ . To derive the analytical solutions we introduce a cylindrical coordinate system  $(r, \phi)$  centered in  $(\bar{x}, \bar{y})$ . Again, we will use the velocity potential introduced in Section 4.2, with the same harmonic time dependence. Hence, we need to solve (16) for  $\Psi(x, y)$  subject to the boundary condition  $\hat{\mathbf{n}} \cdot \nabla \Psi = \partial \Psi / \partial n = 0$  on the cylinder surface.

We assume an incoming wave  $\Psi^0 = e^{ikx} = e^{ikr \cos \phi}$ , and want to solve for  $\bar{\Psi}$  such that  $\Psi = \Psi^0 + \bar{\Psi}$ . In cylindrical coordinates, (16) reads

Table 11

As Table 10 (coefficients **not** modified) but for errors measured in the discrete  $L^2$ -norm

$N$	$u$		$v$		$p$	
	Error	$q$	Error	$q$	Error	$q$
100	0.3433	–	0.2231	–	0.1633	–
300	1.1254	0.92	0.0867	0.86	0.0579	0.94
900	0.0490	0.86	0.0401	0.70	0.0300	0.60

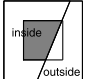


$\alpha = 3\pi/8$   
 $\bar{x}_0 = \frac{3\pi}{2}(2 - 1.01\sqrt{2})$

Table 12

As Table 10 (errors in maximum norm) but for **modified** coefficients

$N$	$u$		$v$		$p$	
	Error	$q$	Error	$q$	Error	$q$
100	1.4477	–	1.5048	–	1.0358	–
300	0.4970	0.97	0.4699	1.06	0.1978	1.51
900	0.1357	1.18	0.1271	1.19	0.0670	0.99

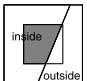


$\alpha = 3\pi/8$   
 $\bar{x}_0 = \frac{3\pi}{2}(2 - 1.01\sqrt{2})$

Table 13

As Table 10 but for **modified** coefficients with errors measured in discrete  $L^2$ -norm

$N$	$u$		$v$		$p$	
	Error	$q$	Error	$q$	Error	$q$
100	0.3263	–	0.1990	–	0.1528	–
300	0.1121	0.97	0.0614	1.07	0.0332	1.39
900	0.0375	1.00	0.0199	1.02	0.0097	1.12



$\alpha = 3\pi/8$   
 $\bar{x}_0 = \frac{3\pi}{2}(2 - 1.01\sqrt{2})$

$$\frac{1}{r} \frac{\partial}{\partial r} \left( r \frac{\partial \Psi}{\partial r} \right) + \frac{1}{r^2} \frac{\partial^2 \Psi}{\partial \phi^2} + k^2 \Psi = 0. \tag{21}$$

The boundary condition  $\partial \Psi / \partial n = 0$  is

$$\left. \frac{\partial \Psi^0}{\partial r} \right|_{r=R} + \left. \frac{\partial \bar{\Psi}}{\partial r} \right|_{r=R} = 0. \tag{22}$$

Particular solutions to (21) are given by

$$\Psi_n^1 = [M_n H_n^{(1)}(kr) + N_n H_n^{(2)}(kr)] \cos n\phi, \quad \Psi_n^2 = [\tilde{M}_n H_n^{(1)}(kr) + \tilde{N}_n H_n^{(2)}(kr)] \sin n\phi,$$

where  $H_n^{(1)}(\xi)$  and  $H_n^{(2)}(\xi)$  are the Hankel functions of order  $n$ , of the first and second kind, respectively. See for example [9]. The problem is symmetric with respect to the  $x$ -axis, and hence an even function of  $\phi$ , and there will be no  $\sin n\phi$  terms in the expansion of  $\bar{\Psi}$ . In addition, the radiation condition



$$\lim_{r \rightarrow \infty} \sqrt{r} \left( \frac{\partial \bar{\Psi}}{\partial r} - ik \bar{\Psi} \right) = 0$$

accepts only outgoing waves, and thus  $N_n = 0$  for all  $n$ .

We have

$$\bar{\Psi}(r, \phi) = \sum_{m=0}^{\infty} M_n H_n^{(1)}(kr) \cos n\phi. \tag{23}$$

For the incoming wave we have the expansion [9],

$$\Psi^0(r, \phi) = e^{ikr \cos \phi} = J_0(kr) + 2 \sum_{n=1}^{\infty} (i)^n J_n(kr) \cos n\phi,$$

where  $J_n(\xi)$  is the Bessel function of order  $n$ . The boundary condition (22) at  $r = R$  determines the coefficients  $M_n$  in the expansion of  $\bar{\Psi}$  (23). We get,

$$M_0 = -\frac{J'_0(kR)}{H_0^{(1)'}(kR)}, \quad M_n = -\frac{2(i)^n J'_n(kR)}{H_n^{(1)'}(kR)}, \quad n = 1, \dots, \infty.$$

With  $\Psi = \Psi_0 + \bar{\Psi}$ , we can evaluate our analytical solutions for  $p, u$  and  $v$  for  $r \geq R$ , using (19). In doing this, the following recursion formulas, that hold both for the Bessel functions  $J_n(\xi)$  and the Hankel functions  $H_n^{(1)}(\xi)$  are useful (again, see [9]):

$$J'_0(\xi) = -J_1(\xi), \quad J'_n(\xi) = -\frac{n}{\xi} J_n(\xi) + J_{n-1}(\xi), \quad n \geq 1.$$

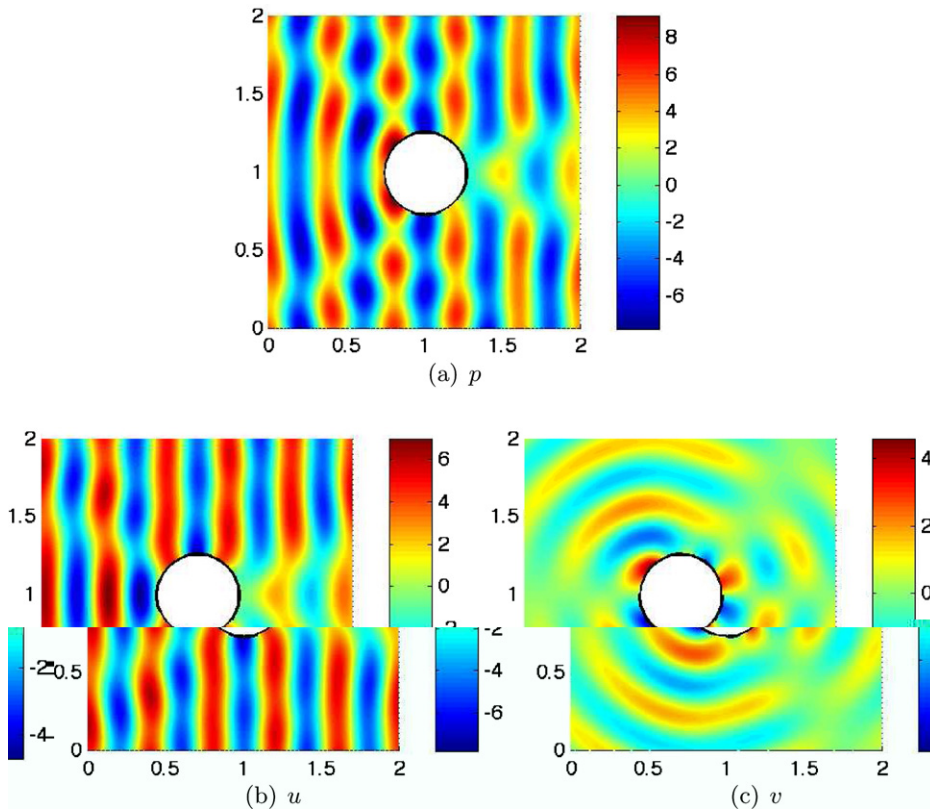


Fig. 13. The analytical solution for  $p, u$  and  $v$  at  $t = 0.3\pi$ . The cylinder location is given by  $(\bar{x}, \bar{y}) = (1 + 1/150, 1 - \sqrt{2}/200)\pi$  and  $R = 4\pi/15$ .

In Fig. 13, we plot the analytical solutions at  $t = 0.3\pi$  for an incoming wave with wave number  $k = 5$ , and  $a = -1$ ,  $b = -1$ , s.t.  $c = 1$ , and hence  $\omega = k$ .

## 5.2. Numerical results

In this section, we present the numerical results for an incoming plane wave that is reflected at a solid cylinder. The numerical parameters are the same as in Section 4.3. Also here, we set  $a = b = -1$  and consider an incoming wave with wave number  $k = 5$ , for which the analytical solutions were plotted in the previous section. The boundary  $\Gamma$  is defined as a circle with radius  $R$ , with the center point  $(\bar{x}, \bar{y})$ . Again, we want to perform simulations for different shifts in the grid. We set  $R = 4\pi/15$  and  $\bar{y} = (1 - \sqrt{2}/200)\pi$ , and we set  $\bar{x}_0 = (1 + 1/150)\pi$  and let  $\bar{x}$  vary over  $M = 6$  shifts in the grid, according to (20). The errors are measured in both maximum norm and the discrete  $L^2$ -norm as compared to the analytical solution over the part of the region  $[\pi/2, 3\pi/2] \times [\pi/2, 3\pi/2]$  that falls inside the physical domain. This is to avoid measuring errors occurring at the outer boundaries. The errors presented in the Tables 14–17 are the largest errors incurred for the  $M = 6$  shifts in the grid.

Table 14  
Error in maximum norm and computed convergence rate  $q$  at  $t = 0.3\pi$  for  $u$ ,  $v$  and  $p$

$N$	$u$		$v$		$p$	
	Error	$q$	Error	$q$	Error	$q$
100	3.4278	–	3.2776	–	2.1158	–
300	2.8908	0.16	2.8489	0.13	0.7881	0.90
900	3.3326	–0.13	3.5508	–0.20	0.5304	0.36

The coefficients have **not** been modified. Error given is taken as the maximum over  $M = 6$  shifts of  $\bar{x}$  according to (20).  $R = 4\pi/15$  and  $(\bar{x}_0, \bar{y}) = (1 + 1/150, 1 - \sqrt{2}/200)\pi$ .

Table 15  
As Table 14 (coefficients **not** modified) but for errors measured in the discrete  $L^2$ -norm

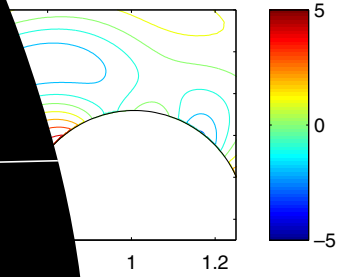
$N$	$u$		$v$		$p$	
	Error	$q$	Error	$q$	Error	$q$
100	0.3479	–	0.2208	–	0.3416	–
300	0.1266	0.92	0.0992	0.73	0.1092	1.04
900	0.0578	0.71	0.0512	0.60	0.0487	0.74

Table 16  
As Table 14 (errors in maximum norm) but for **modified** coefficients

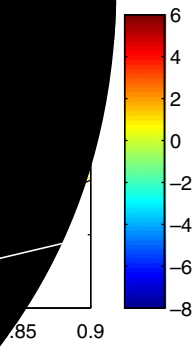
$N$	$u$		$v$		$p$	
	Error	$q$	Error	$q$	Error	$q$
100	1.8666	–	1.9906	–	1.9555	–
300	0.5872	1.05	0.5942	1.10	0.4451	1.35
900	0.1992	0.98	0.2138	0.93	0.1367	1.07

Table 17  
As Table 14 but for **modified** coefficients with errors measured in discrete  $L^2$ -norm

$N$	$u$		$v$		$p$	
	Error	$q$	Error	$q$	Error	$q$
100	0.3138	–	0.2130	–	0.3430	–
300	0.1000	1.04	0.0573	1.20	0.0973	1.15
900	0.0333	1.00	0.0186	1.03	0.0300	1.07



$\theta/\pi$   
 coefficients **modified**.



**modified**.

shown in Fig. 15.

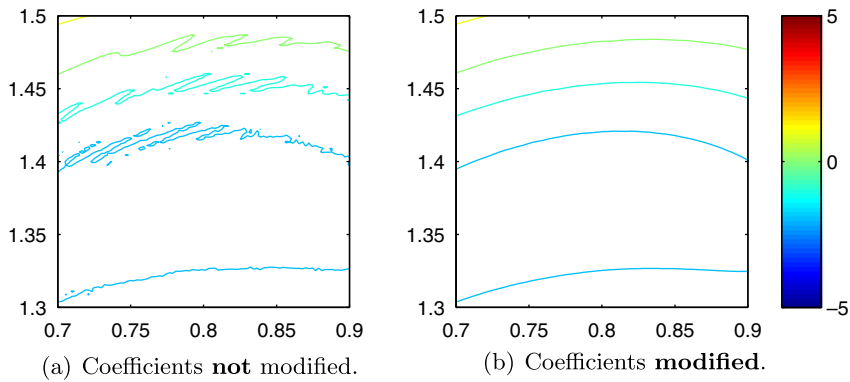


Fig. 18. Close-ups of the numerical solutions for  $v$  shown in Fig. 16.

In Figs. 14–16 analytical and numerical results for  $p$ ,  $u$  and  $v$  are shown, and a close-up of the numerical solutions for  $u$  and  $v$  are shown in Figs. 17 and 18. We can note that with the original stair-cased approximation, the numerical solution is of visibly lower quality in terms of numerical oscillations compared to when the coefficients are modified. This is especially true for  $v$ , which holds no contribution from the incoming wave, but only from the reflected outgoing wave.

## 6. Conclusions

A new set of boundary conditions for the Yee scheme in two-dimensions on structured grids is presented. The conditions are of the same simple form as the so-called stair-case boundary conditions for general geometries and the modification fits well into the structure of existing Yee codes. We show that the standard stair-case conditions give local  $O(1)$  errors in many cases but our new conditions are consistent and result in first order convergence rate. Furthermore the new numerical solutions do not show the same numerical grid oscillations as solutions based on the stair-case conditions. The CFL condition for the new scheme is the same as that for the Yee scheme without boundaries, and hence the new scheme retains the full efficiency of the Yee scheme.

The boundary technique introduced in this paper extends formally to three dimensions, but more investigations are needed to consider the practical details.

## Acknowledgements

AKT acknowledges support from DOE Grant DE-FG02-88ER25053 and an Alfred P. Sloan Research Fellowship. AKT is also a Royal Swedish Academy of Sciences Research Fellow supported by a grant from the Knut and Alice Wallenberg Foundation. BE acknowledges support from the Swedish Foundation for Strategic Research.

## Appendix.

For each case of the intersections depicted in Figs. 4 and 5, we only need to modify one coefficient to fulfill the consistency condition, given in Table 1. Which coefficient we choose to modify depends on the case, and the angle  $\alpha$ . The modified coefficient for all cases is listed in Tables 18 and 19. The form of the factor in the modification, combined with the range of  $\alpha$ , ensures that each modified coefficient can be written as  $\beta \cdot a$ , where  $0 \leq \beta \leq 1$ . This gives a sound implementation with the original bounds on the coefficients. As we have seen in numerical experiments (Section 3.2), the resulting scheme has a CFL condition that is the same as for the original Yee scheme without boundaries.

The angle  $\alpha$  is the angle to the  $x$ -axis of the line tangent to the boundary at the point  $(x^*, y^*)$  ( $0 \leq \alpha < \pi$ ), where the point  $(x^*, y^*)$  can be any point on the boundary within the  $h \times h$  square defined by the computa-

Table 18

The table gives the one coefficient in the approximation (9) that is modified for each case of intersection depicted in Fig. 4

Case	Range of $\alpha$	Coefficient modified
XY1	$\alpha \in [0, \pi/4]$	$\tilde{a}^E = \frac{\sin \alpha}{\cos \alpha} a$
	$\alpha \in (\pi/4, \pi/2]$	$\tilde{a}^S = \frac{\cos \alpha}{\sin \alpha} a$
XY2	$\alpha \in [\pi/2, 3\pi/4]$	$\tilde{a}^S = \frac{\cos \alpha}{\sin \alpha} a$
	$\alpha \in (3\pi/4, \pi)$	$\tilde{a}^W = \frac{\sin \alpha}{\cos \alpha} a$
XY3	$\alpha \in [\pi/2, 3\pi/4]$	$\tilde{a}^N = -\frac{\cos \alpha}{\sin \alpha} a$
	$\alpha \in (3\pi/4, \pi)$	$\tilde{a}^E = -\frac{\sin \alpha}{\cos \alpha} a$
XY4	$\alpha \in [0, \pi/4]$	$\tilde{a}^W = -\frac{\sin \alpha}{\cos \alpha} a$
	$\alpha \in (\pi/4, \pi/2]$	$\tilde{a}^N = -\frac{\cos \alpha}{\sin \alpha} a$

With these modifications, the consistency conditions given in Table 1 are fulfilled.

Table 19

The table gives the one coefficient in the approximation (9) that is modified for each case of intersection depicted in Fig. 5

Case	Range of $\alpha$	Coefficient modified
X1	$\alpha \in [\pi/4, \pi/2]$	$\tilde{a}^N = (1 - \frac{\cos \alpha}{\sin \alpha}) a$
	$\alpha \in (\pi/2, 3\pi/4]$	$\tilde{a}^S = (1 + \frac{\cos \alpha}{\sin \alpha}) a$
X2	$\alpha \in [\pi/4, \pi/2]$	$\tilde{a}^S = (1 - \frac{\cos \alpha}{\sin \alpha}) a$
	$\alpha \in (\pi/2, 3\pi/4]$	$\tilde{a}^N = (1 + \frac{\cos \alpha}{\sin \alpha}) a$
Y1	$\alpha \in [0, \pi/4]$	$\tilde{a}^W = (1 - \frac{\sin \alpha}{\cos \alpha}) a$
	$\alpha \in [3\pi/4, \pi)$	$\tilde{a}^E = (1 + \frac{\sin \alpha}{\cos \alpha}) a$
Y2	$\alpha \in [0, \pi/4]$	$\tilde{a}^E = (1 - \frac{\sin \alpha}{\cos \alpha}) a$
	$\alpha \in [3\pi/4, \pi)$	$\tilde{a}^W = (1 + \frac{\sin \alpha}{\cos \alpha}) a$

With these modifications, the consistency conditions given in Table 1 are fulfilled.

tional stencil. If the boundary  $\Gamma$  is a straight line cutting through the grid,  $\alpha$  is naturally given by the angle of that line to the  $x$ -axis. If  $\Gamma$  is curved, a point  $(x^*, y^*)$  on  $\Gamma$  must be selected, and  $\alpha$  for the tangent line at that point computed. Here, we have a freedom in which point on the curve that we select. In some cases, the tangent angle  $\alpha$  will not be within the appropriate bounds (Tables 18 and 19) for all possible choices of  $(x^*, y^*)$ . However, it is always possible to select a point  $(x^*, y^*)$  such that it is.

For cases XY1 and XY4, we compute  $(x^*, y^*)$  as the intersection of  $\Gamma$  and the line running through  $(x_{j+1/2}, y_{l+1/2})$  with a slope of  $-1$ . For cases XY2 and XY3, we do the same, but using a line with a slope of 1. Assuming that the boundary is smooth, and that its curvature is not too high relative to the grid resolution, this will yield values of  $\alpha$  within the appropriate range given in Table 18.

When the stencil is only intersected in  $x$  (case X1 and X2), we take  $y^* = y_{l+1/2}$  and compute  $x^*$  as the point where  $\Gamma$  intersects this horizontal line. Correspondingly, for case Y1 and Y2, we let  $x^* = x_{j+1/2}$  and compute  $y^*$ . For these cases, where the stencil is cut only in  $x$  or  $y$ , it is however possible that  $\alpha$  for the selected  $(x^*, y^*)$  falls outside of the appropriate range, as given in Table 19. We then use an alternate strategy, as used in the cases where the stencil is cut both in  $x$  and  $y$ , to compute a new  $(x^*, y^*)$  and corresponding  $\alpha$ .

## References

- [1] A.C. Cangellaris, D.B. Wright, Analysis of the numerical error caused by the stair-stepped approximation of a conducting boundary in FDTD simulations of electromagnetic phenomena, IEEE Trans. Antenn. Propagat. 39 (1991) 1518–1525.
- [2] S. Dey, R. Mitra, A locally conformal finite-difference time-domain (FDTD) algorithm for modeling three-dimensional perfectly conducting objects, Microwave Guided Wave Lett. 7 (1997) 273–275.
- [3] A. Ditkowski, K. Dridi, J.S. Hesthaven, Convergent cartesian grid methods for Maxwell's equations in complex geometries, J. Comput. Phys. 170 (2001) 39–80.
- [4] B. Gustafsson, The convergence rate for difference approximations to mixed initial boundary value problems, Math. Comput. 29 (1975) 396–406.
- [5] B. Gustafsson, P. Wahlund, Time compact high order difference methods for wave propagation, 2-D, J. Sci. Comput. 25 (2005) 195–211.
- [6] Y. Hao, C.J. Railton, Analyzing electromagnetic structures with curved boundaries on cartesian FDTD meshes, IEEE Trans. Microw. Theory Tech. 46 (1998) 82–88.

- [7] R. Holland, Pitfalls of staircase meshing, *IEEE Trans. Electromagn. Compat.* 35 (1993) 434–439.
- [8] T.G. Jurgens, A. Taflove, K. Umashankar, T.G. Moore, Finite difference time-domain modeling of curved surfaces, *IEEE Trans. Antenn. Propagat.* 40 (1992) 357–366.
- [9] N.N. Lebedev, *Special Functions and their Applications*, Dover Publications, 1972.
- [10] P. Monk, *Finite Element Methods for Maxwell's Equations*, Oxford University Press, 2003.
- [11] C.J. Railton, J.B. Schneider, An analytical and numerical analysis of several locally conformal FDTD schemes, *IEEE Trans. Microw. Theory Tech.* 47 (1999) 56–66.
- [12] Y.S. Rickard, N.K. Nikolova, Off-grid perfect boundary conditions for the FDTD method, *IEEE Trans. Microw. Theory Tech.* 53 (2005) 2274–2283.
- [13] T. Rylander, A. Bondeson, Stable FEM-FDTD hybrid method for Maxwell's equations, *Comput. Phys. Commun.* 125 (2000) 75–82.
- [14] A. Taflove, S.C. Hagness, *Computational Electrodynamics: The Finite Difference Time Domain Method*, third ed., Artech House, 2005.
- [15] A.K. Tornberg, B. Engquist, Regularization for accurate numerical wave propagation, *Methods Appl. Anal.* 13 (2006) 247–274.
- [16] A.K. Tornberg, B. Engquist, B. Gustafsson, P. Wahlund, A new type of boundary treatment for wave propagation, *BIT* 46 (2006) s145–s170.
- [17] T. Xiao, Q.H. Liu, Enlarged cells for the conformal FDTD method to avoid the time step reduction, *IEEE Microw. Wireless Compon. Lett.* 14 (2004) 551–553.
- [18] T. Xiao, Q.H. Liu, A staggered upwind embedded boundary (SUEB) method to eliminate the FDTD staircasing error, *IEEE Trans. Antenn. Propagat.* 52 (2004) 730–741.
- [19] K.S. Yee, Numerical solution of initial boundary value problems involving Maxwell's equations in isotropic media, *IEEE Trans. Antenn. Propagat.* 14 (1966) 302–307.
- [20] I.A. Zagorodnov, R. Schuhmann, T. Weiland, A uniformly stable conformal FDTD-method in Cartesian grids, *Int. J. Numer. Model.* 16 (2003) 127–141.